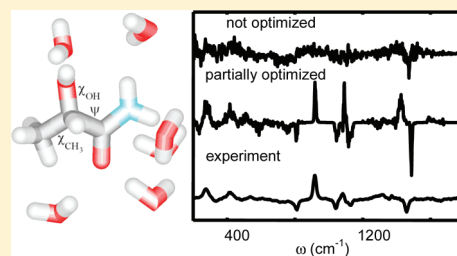


Correction of Vibrational Broadening in Molecular Dynamics Clusters with the Normal Mode Optimization Method

Jana Hudecová,^{†,‡} Kathrin H. Hopmann,[§] and Petr Bourčič,^{*,†}[†]Institute of Organic Chemistry and Biochemistry, Academy of Sciences, Flemingovo nám. 2, 166 10 Prague, Czech Republic[‡]Institute of Physics, Charles University, Ke Karlovu 5, 12116 Prague 2, Czech Republic[§]Department of Chemistry, Centre for Theoretical and Computational Chemistry, University of Tromsø, N-9037 Tromsø, Norway

ABSTRACT: Vibrational properties of solutions are frequently simulated with clusters of a solute and a few solvent molecules obtained during molecular dynamics (MD) simulations. The raw cluster geometries, however, often provide unrealistic vibrational band broadening, for both *ab initio* and empirical force fields. In this work, partial optimization in normal-mode coordinates is used on empirical basis to reduce the broadening. The origin of the error is discussed on a simplified two-dimensional system, which indicates that the problem is caused by the anharmonic MD potential, mode coupling, and neglect of quantum effects. Then the procedure of partial geometry optimization on Raman and Raman optical activity (ROA) spectra is applied and analyzed for the solvated lactamide molecule. Comparison to experiment demonstrates that the normal-mode partial optimization technique with a suitable frequency limit can significantly reduce the broadening error. For lactamide, experimental and simulated vibrational bandwidths are compared; the most realistic theoretical spectra are obtained for partially optimized clusters with the vibrational wavenumber cutoff of about 200 cm^{-1} .



INTRODUCTION

Computations of solution properties with clusters containing explicit solvent molecules became popular because of the superior results to vacuum or simpler polarizable continuum models (PCM),^{1–4} availability of accurate molecular dynamics (MD) force fields,⁵ feasible *ab initio* dynamical schemes,^{6–8} and the steady increase of computer power. For example, we found that the explicit solvent model is needed to accurately simulate NMR parameters of solvated molecules,^{4,9} and polarized continuum models (PCM) are often inadequate to describe hydrogen bonding or temperature effects on the vibrational properties of the peptide amide group.^{10,11}

In vibrational spectroscopy, a combination of quantum and molecular dynamics methods is often needed in larger cluster computations to calculate realistic band shapes. In particular, polar molecules, such as peptide models, exhibit large inhomogeneous band broadening, for example in IR,^{12,13} VCD,¹⁴ or two-dimensional^{15,16} (2D) spectroscopic techniques. The band-shape modeling lends the peptide vibrational spectroscopy an enhanced structural sensitivity. This mostly originates from vibrational coupling among the individual amide chromophores, resulting in delocalized modes, which can give rise to complex, asymmetric band shapes.^{17,18} For example, β -sheet peptide conformations exhibit different IR band shape of the carbonyl stretching mode than α -helices. The solvent has also a dramatic effect on the amide and other vibrational frequencies.^{19,20} In the vibrational optical activity techniques,²¹ the structural sensitivity enhancement is mostly achieved through the spectral sign pattern.^{22,23} Nevertheless, for the case of flexible and polar molecule with many overlapping transitions, the band-shape modeling with explicit solvent is also necessary.²⁴

The instantaneous normal-mode approximation investigated in the present study provides a convenient way to compute the vibrational frequencies and intensities for the condensed phase at the harmonic level.²⁵ Second energy derivatives and the harmonic vibrations are estimated with MD snapshot geometries. While such approach is a useful approximation for some liquids,^{26,27} in a recent study²⁸ we observed unrealistic inhomogeneous broadening of simulated Raman and Raman optical activity (ROA) bands when raw clusters were used to simulate two hydrated molecules, lactamide and 2-aminopropan-1-ol. The problem persisted both for classical MD or Car–Parrinello molecular dynamics (CPMD)⁶ snapshots.

For completeness, we should also mention the time-dependent approaches of band-shape generation, frequently used to model vibrational linear or 2D spectra.^{15,29} These are based on the semiclassical line-shape theory, and the line width is controlled through a phenomenological decay function.^{30,31} In a static averaging approximation, for example, the absorption profile is calculated from individual MD snapshots and the resultant electrostatic potentials.¹³ This typically leads to too broad bands, which can be improved by many techniques,³² discussion of which goes beyond the scope of this work.

But also in the instantaneous normal-mode approximation, most coordinates are too dispersed if compared to quantum-mechanical uncertainty, as the MD cluster geometries are based on classical mechanics. We therefore propose to efficiently

Received: September 12, 2011

Revised: October 21, 2011

Published: December 01, 2011

reduce the consequent spectral broadening by a partial optimization of the cluster geometries.^{11,28} In particular, the normal-mode optimization algorithm³³ seems to be very suitable for this purpose, as it was found particularly robust for clusters,³⁴ it is numerically stable, and it does not require manual definition of the coordinates. For larger molecules, for example, we used it to fix the desired conformations of peptides³⁵ and large DNA³⁶ molecules, whereas the normal mode's degrees of freedom important for the spectrum could be relaxed.

For the clusters investigated in the present study, the extent of the partial optimization is crucial for realistic results. The geometry of MD clusters cannot be optimized completely to avoid collapse to an energy minimum, implying a loss of the structural information obtained by the dynamics. In the normal-mode partial optimization, this can be controlled by a sole parameter, the maximal harmonic normal-mode frequency (ω_{\max}), below which the normal modes are fixed. By fixing the shallow modes, such motions as molecular translations and rotations are restricted. However, the limit has been used on an ad hoc basis so far. In particular, neither the relation of ω_{\max} to the resulting bandwidths nor the effect on molecular coordinates has been established. To rationalize the choice of this parameter, in this study we perform Raman spectral simulation based on 100 snapshots of lactamide in a box of water molecules obtained previously by a CPMD simulation,²⁸ and monitor the resultant inhomogeneous broadening. The coordinate changes occurring during the partial optimization were monitored, and the simulated bandwidths were compared to experimental Raman spectra.

To better understand the origin of the broadening in the instantaneous normal-mode approximation, we also constructed a model two-dimensional system, where the classical MD results could be compared to benchmark vibrational configuration interaction (VCI) computation. As shown below, already the model 2D Hamiltonian exhibits band broadening; this is primarily caused by the anharmonic character of the potential and coupling of the vibrational modes. However, the results on the lactamide also document that the error can be efficiently reduced by the partial optimization, and that this empirical procedure can be at least partially justified by physical arguments. In particular, the low-frequency vibrations (solvent translations, torsions, etc.) that are temperature-excited are treated classically, using the MD coordinate dispersion, whereas higher-energy vibrations (bending and stretching modes) need to be fully optimized.

METHODS

A Model of the Anharmonic Coupling. To obtain a deeper insight into the role of anharmonicities in MD potential and spectra calculated within the instantaneous normal-mode approximation, we considered a two-dimensional model system with a potential $V = (\omega_1/2)q_1^2 + (\omega_2/2)q_2^2 + (d_{1122}/24)q_1^2q_2^2$, where q_i denote the dimensionless normal-mode coordinates³⁷ and cm^{-1} are used as energy units. The harmonic parameters were inspired by a B3LYP³⁸/6-31G** computation³⁹ of a hydrogen-bonded water dimer,¹⁰ with the frequencies $\omega_1 = 28 \text{ cm}^{-1}$ and $\omega_2 = 3712 \text{ cm}^{-1}$ corresponding to a water wagging and OH stretching mode, respectively. By choice we wanted to mimic a coupling of low ($\omega \ll kT$, where kT is the Boltzmann quantum) and high ($\omega \gg kT$) frequency modes. The quartic anharmonic constant was set to $d_{1122} = 448 \text{ cm}^{-1}$. The constant was chosen rather arbitrarily; nevertheless, its magnitude corresponds to usual anharmonic coupling constants in molecules.⁴⁰

To mimic the MD procedure, the classical instantaneous spectra were simulated for 90×90 coordinates equidistantly chosen on the 2D $q_1 \times q_2$ potential energy surface, within $q_{\min} = -2$ and $q_{\max} = 2$. At each point an effective MD frequency of the second mode was calculated as a second derivative of the potential, $\omega_2' = \partial^2 V / \partial q_2^2$. The resulting spectral band was weighted by the corresponding Boltzmann factor for 50 and 300 K. An arbitrary dipole strength was introduced, constant within the coordinate space. Individual transitions were summed and convoluted with Lorentzian band 10 cm^{-1} wide (full widths at half-height, fwhh) to smooth the resultant curve.

For the same system, quantum transition frequencies were obtained by vibrational configuration interaction (VCI)⁴¹ done in the harmonic oscillator basis involving 51 states, and the spectrum was generated similarly as for the classical case using Boltzmann weighting of the initial states. For the first and second normal mode, 10 and 5 times excited states were included, respectively. The S4 program⁴² was used for the VCI computation. A constant intensity of the $|00\rangle \rightarrow |01\rangle$ transition was assumed, similarly as for the MD model; i.e., the intensity anharmonicities (second dipole derivatives) were neglected.

Normal-Mode Optimization. In the vicinity of an energy minimum, we can introduce a molecular harmonic vibrational Hamiltonian given in a matrix form by³⁷

$$H = \frac{1}{2} (\Delta \dot{\mathbf{x}}^t \mathbf{M} \Delta \dot{\mathbf{x}} + \Delta \mathbf{x}^t \mathbf{f} \Delta \mathbf{x}) \quad (1)$$

where \mathbf{M} is diagonal matrix of atomic masses m_i , $\Delta \mathbf{x}$ is the vector of atomic displacements with respect to the equilibrium positions, $\Delta x_i = x_i - x_i^0$, superscript t denotes transpose matrices, and \mathbf{f} is the Cartesian force field. Conveniently, mass-weighted coordinates are introduced as $X_i = (m_i)^{1/2} \Delta x_i$, so that $f_{ij} = (m_i m_j)^{1/2} F_{ij}$, and $H = 1/2 (\dot{\mathbf{X}}^t \mathbf{X} + \mathbf{X}^t \mathbf{F} \mathbf{X})$. Finally, the normal-mode coordinates Q_i are typically introduced by

$$\mathbf{X} = \mathbf{s} \mathbf{Q} \quad (2)$$

where the transformation matrix satisfies $\mathbf{s}^t \mathbf{s} = \mathbf{1}$, $\mathbf{s}^t \mathbf{F} \mathbf{s} = \mathbf{\Lambda}$; $\mathbf{1}$ is the unit matrix, and $\mathbf{\Lambda}$ is a diagonal matrix ($\Lambda_{ij} = \omega_i^2 \delta_{ij}$) containing squares of the normal-mode frequencies ω_i . The Hamiltonian then becomes a sum of harmonic oscillators:

$$H = \sum_i \frac{1}{2} (\dot{Q}_i^2 + \omega_i^2 Q_i^2) \quad (3)$$

Equation 3 is usually used to obtain vibrational molecular energies. However, using the linear transformation between the Cartesian displacements and the normal-mode coordinates

$$\Delta x_\mu = \sum_i \frac{1}{\sqrt{m_\mu}} s_{\mu i} Q_i = \sum_i S_{\mu i} Q_i \quad (4)$$

we can use the Q_i coordinates during the optimization in place of the more usual internal redundant^{43,44} or Cartesian coordinates. In the QGRAD⁴⁵ program interfaced to Gaussian,³⁹ initial Cartesian force field can be estimated on a lower level, and it is continuously updated by the "BGFS"⁴⁶⁻⁴⁹ formula from Cartesian gradients

$$\mathbf{f}^{(i+1)} = \mathbf{f}^{(i)} - \left(\frac{\Delta \mathbf{g}^t \Delta \mathbf{g}}{\Delta \mathbf{x}^t \Delta \mathbf{g}} + \frac{(\mathbf{f}^{(i)} \Delta \mathbf{x})^t \Delta \mathbf{x} \mathbf{f}^{(i)}}{\Delta \mathbf{x}^t \mathbf{f}^{(i)} \Delta \mathbf{x}} \right) \quad (5)$$

where $\Delta \mathbf{g}$ and $\Delta \mathbf{x}$ are gradient and coordinate increments between the steps i and $i + 1$.

The actual optimization is performed in normal modes, using the RFO^{50–54} updating. New normal-mode displacements are

$$d\mathbf{Q}^{(i+1)} = -\frac{2\mathbf{g}^{(i)}}{\Lambda_{ii} + \sqrt{\Lambda_{ii}^2 + 4(\mathbf{g}^{(i)})^2}} \quad (6)$$

so that updated Cartesian coordinates may be obtained as $\mathbf{x}^{(i+1)} = \mathbf{x}^{(i)} - \mathbf{S}d\mathbf{Q}^{(i+1)}$. Further details can be found in the previous works.^{33,34} Note that this scheme also enables a full optimization of the system. In the restricted normal-mode optimization adopted in this work, some modes (with $\omega_i \in (\omega_{\min}, \omega_{\max})$) are kept constant ($dQ_i = 0$).

Lactamide Raman and ROA Spectra. The geometry CPMD snapshots were selected randomly from a 48 ps simulation performed previously.²⁸ From the snapshots, clusters containing (S)-lactamide and 3–9 hydrogen-bonded waters closer than 3.6 Å to a lactamide atom were selected. This approximation well included the effect of the first hydration shell on the vibrational properties of lactamide; more distant water molecules did not influence the signal significantly. All computations were performed at the B3LYP/6-311++G**/CPCM level of theory, using the continuum model to simulate the effect of the more distant waters, not explicitly included in the computations. The constrained normal-mode optimization was repeated for seven values of ω_{\max} : 10, 20, 50, 100, 200, 300, and 600 cm^{-1} . In addition, we also studied the raw nonoptimized CPMD snapshots corresponding to infinite ω_{\max} . To fix large imaginary frequencies occasionally exhibited by some CPMD geometries, a lower limit $\omega_{\min} = -300 \text{ cm}^{-1}$ was introduced and kept constant.

For the $8 \times 100 = 800$ optimized and raw geometries, Raman backscattered line intensities⁵⁵ were calculated by Gaussian, and the water signal (corresponding polarizability derivatives) was deleted. Smoother spectra were generated by summing the 100 cluster signals and performing a convolution (e.g., ref 56, eq 3) with Lorentzian bands 2 cm^{-1} wide, which were much narrower than the inhomogeneous broadening.

For selected lactamide vibrational bands (528, 813, and 920 cm^{-1}), theoretical bandwidths (fwhh) were obtained from the simulated spectra by fitting with Lorentzian bands. The bands were chosen at frequencies where overlap of multiple vibrational transitions was minimal, and the fitting with the symmetric function was reasonable. By comparing whole spectral shapes, we deduce that their broadening reflects behavior of the spectral signals within the entire range of frequencies. For the fitting, we used an iterative procedure, comparing integral mean quadratic deviations of spectral intensities with the ideal Lorentzian profile.

RESULTS AND DISCUSSION

Two-Dimensional Model. The simpler 2D model Hamiltonian well documents the limits of the instantaneous normal-mode approximation used in MD. In Figure 1, absorption spectra are simulated for the two-dimensional model using the classical and quantum approach. We can already see some common errors introduced by the classical approximation. First, the quantum theory provides a few transitions only, whereas the classical approach generates a continuous spectrum (approximated by the high line density corresponding to the coordinate grid). This is apparent namely for the lower temperature (50 K, upper part of Figure 1), where even the lowest energy vibration (with the frequency ω_1) predominantly remains in the ground state, and VCI provides one transition only. For 300 K (lower part of Figure 1)

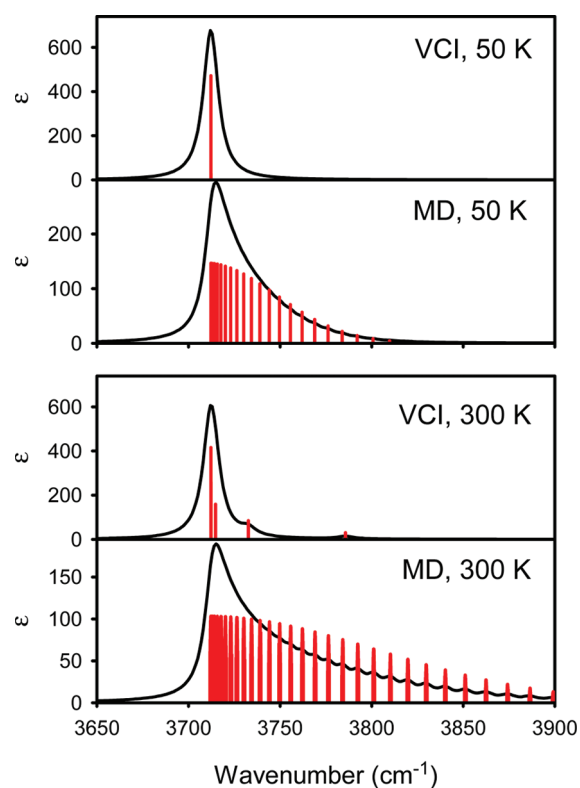


Figure 1. Absorption spectra (ϵ , in arbitrary units) of the 2D model simulated by the quantum (VCI) and classical (MD) approaches at 50 and 300 K.

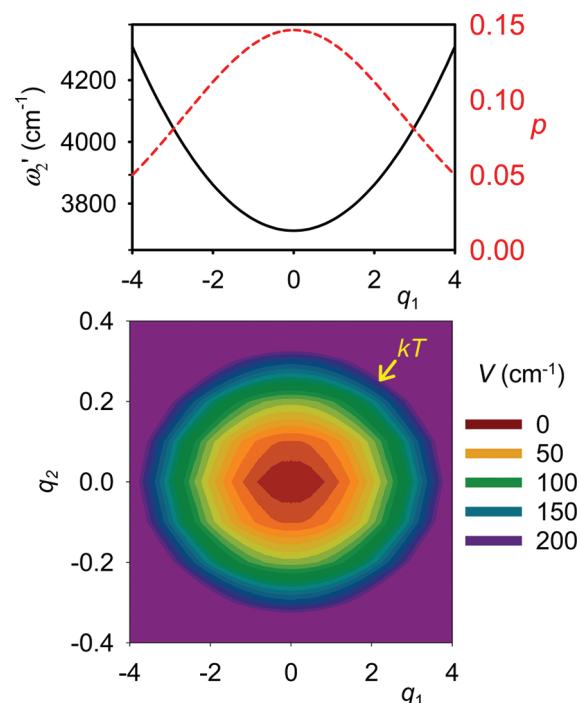


Figure 2. Model 2D potential (bottom, $V = (\omega_1/2)q_1^2 + (\omega_2/2)q_2^2 + (d_{1122}/24)q_1^2q_2^2$, approximate accessible energy at 300 K is indicated by kT), effective harmonic frequency of the second mode $\omega_2' = \partial^2 V / \partial q_2^2$ and Boltzmann probability p for 300 K as dependent on q_1 (top).

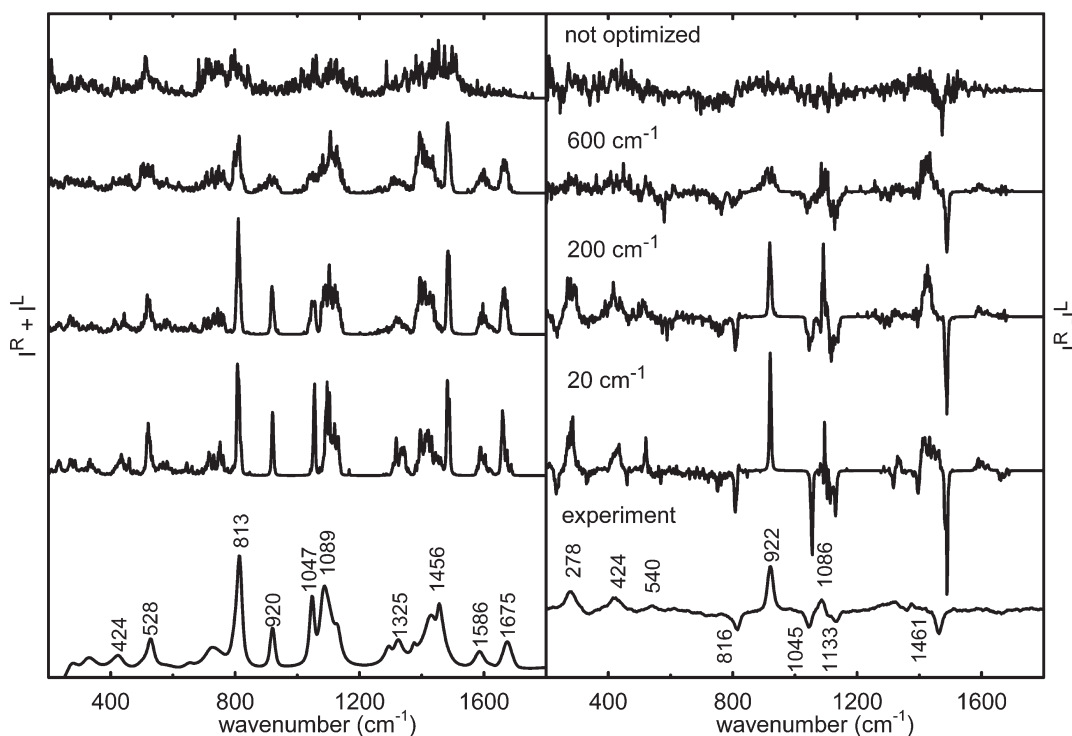


Figure 3. Lactamide solution backscattered Raman (left, $I^R + I^L$) and ROA (right, $I^R - I^L$) spectra simulated with the partially optimized CPMD clusters. The ω_{\max} cutoffs and the experimental spectrum in H_2O with positions of principal peaks are indicated.

more quantum transitions appear; the system starts to exhibit the classical distribution of vibrational frequencies.

The MD spectral shape in Figure 1 can be easily understood on the basis of the potential analyzed in Figure 2. We see that the “molecule” can explore a relatively large part of the potential energy surface, limited approximately by the Boltzmann kT limit. Consequently, different harmonic frequencies equal to the potential second derivatives are obtained for the higher-frequency mode (q_2). For our coupling term, the effective MD frequencies are limited by the lower limit for $q_1 = 0$, i.e., $\omega_2' \geq \omega_2$. However, in the adiabatic quantum model, for $\hbar\omega_2 \gg kT$, only one transition frequency (for 50 K, Figure 1) or a transition with limited number of satellite bands (300 K, Figure 1) is possible.

Another quantum effect, the shift of the maximal frequency, is quite small (1 cm^{-1} , Figure 1), and can be neglected in this case. However, it can be quite large in real molecules,⁵⁷ and except for a partial diagonal correction it cannot be simulated within the instantaneous normal-mode and harmonic schemes. Finally, even for the higher temperature of 300 K the classical bandwidth based on the MD/instantaneous normal-mode approach is still larger than those obtained by the more rigorous VCI calculation.

The example potential was chosen to be simple to enable the benchmark VCI computation. For real systems, we can expect that other anharmonic contributions not included in the simplified 2D Hamiltonian, such as diagonal and cubic terms,⁵⁷ would lead to a more complicated behavior. The 2D model is thus not able to fully explain the MD broadening effects in large clusters; nevertheless, it convincingly indicates that anharmonic coupling terms in the vibrational Hamiltonian cause significant differences between the quantum (VCI) and classical (MD) results.

Solvated Lactamide. Also in the lactamide spectra direct exploitation of MD geometries leads to overestimation of the broadening and quite unrealistic spectral shapes. The spectra

simulated from the raw snapshots, the optimized snapshots with ω_{\max} of 600 , 200 , and 20 cm^{-1} , and the experimental²⁸ spectra measured in aqueous solution are compared in Figure 3 (left, Raman; right, Raman optical activity, ROA). Clearly, the results for raw nonoptimized clusters (top in Figure 3) are unusable for a detailed assignment of the lactamide bands. Similarly as for the model system (Figure 1), the raw MD instantaneous normal-mode approach overestimates the anharmonic force field terms and causes too wide dispersion of the harmonic frequencies.

On the other hand, the partial optimization of cluster geometries leads to a radical improvement. For $\omega_{\max} = 600 \text{ cm}^{-1}$ many of the experimental intensity features for wavenumbers above 800 cm^{-1} are reproduced (Figure 3). However, the bands are still too broad, and no improvement is apparent below 600 cm^{-1} . The Raman band at $\sim 528 \text{ cm}^{-1}$ became even broader for $\omega_{\max} = 600 \text{ cm}^{-1}$ than for the nonoptimized case, which can be explained by the coupling of the complicated 528 cm^{-1} vibrations with higher-frequency modes. For $\omega_{\max} = 200 \text{ cm}^{-1}$ (Figure 3), most of the Raman and ROA intensity features are well developed, and the bandwidths are realistic within the entire wavenumber region. For $\omega_{\max} = 20 \text{ cm}^{-1}$ individual bands can be recognized as well, but most bandwidths become too narrow if compared to the experiment. $\omega_{\max} = 10 \text{ cm}^{-1}$ (not shown) provided virtually the same spectra as $\omega_{\max} = 20 \text{ cm}^{-1}$. Note that simulations in vacuum or a continuum solvent model would provide line spectra only, without any information about the broadening.

The optimizations with too low ω_{\max} become less economic in terms of the required computer time. Note that the normal-mode coordinates, similar to Cartesian coordinates, are in general not suitable for complete molecular optimizations as they do not follow the covalent bond network.³⁴ Thus, whereas the optimization of 100 clusters (without the frequency calculation)

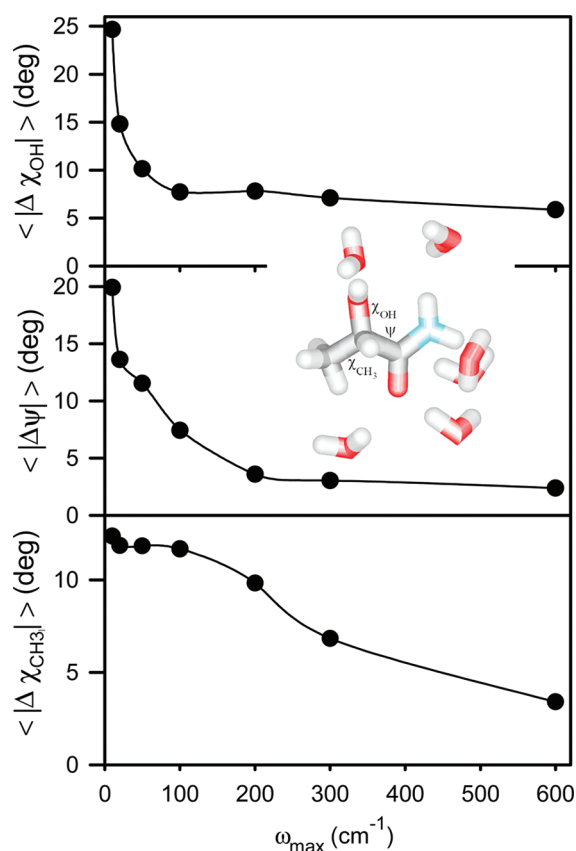


Figure 4. Average absolute changes of three (*S*)-lactamide torsional angles during the optimization, as obtained for seven values of ω_{max} . The averages were obtained from 100 CPMD clusters; the angles $\chi_{\text{OH}} = \angle(\text{C}=\text{O}\text{COH})$, $\psi = \angle(\text{NCCC})$, and $\chi_{\text{CH}_3} = \angle(\text{CCCH})$ are indicated in the randomly chosen snapshot.

required 28 days of CPU time (3 GHz, Intel S160) for the 600 cm^{-1} limit, 89 and 212 days were needed for 200 and 20 cm^{-1} , respectively. We also attempted a full optimization of the clusters, which provided results very close to those obtained with the lowest ω_{max} limits (10 and 20 cm^{-1}). However, many clusters could not be fully optimized because of a lack convergence of the optimization algorithm. The full geometries also do not reflect well the desired dynamical geometry distribution at 300 K ; therefore, we do not include these results in the analysis.

The effect of the optimization limit on the relaxation of molecular coordinates is documented in Figure 4. Here, average changes of the χ_{OH} , ψ , and χ_{CH_3} torsional angles are plotted for seven ω_{max} values. The OH rotation is associated with the shallowest potential, and thus remains fixed for most of the optimization models. The rotation is released for $\omega_{\text{max}} < 100 \text{ cm}^{-1}$, when the change increases steeply. The ψ angle responds more gradually, and it is starting to change already for $\omega_{\text{max}} < 300 \text{ cm}^{-1}$. The CH_3 rotation exhibits the most developed sigmoidal “melting” pattern with a transition frequency at about 250 cm^{-1} . This value also well corresponds to the harmonic normal-mode frequency of this motion.²⁸

A detailed coordinate dispersion is documented on the ψ and χ_{OH} angles in Figure 5. For 10 randomly selected clusters the optimized torsional angles were extracted for each value of ω_{max} . During the optimization, the original broad distribution of ψ (within $\sim 105^\circ$ – 150° for the selected clusters) becomes

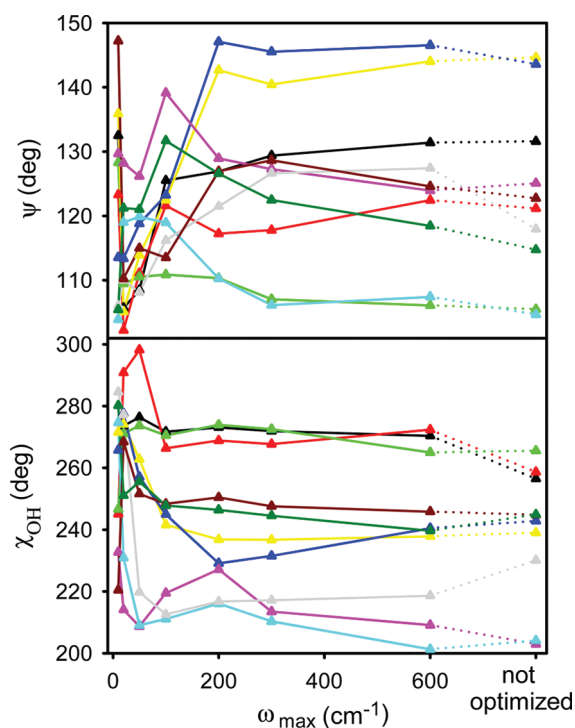


Figure 5. Dependence of the optimized (*S*)-lactamide ψ and χ_{OH} angles on ω_{max} in 10 randomly chosen clusters.

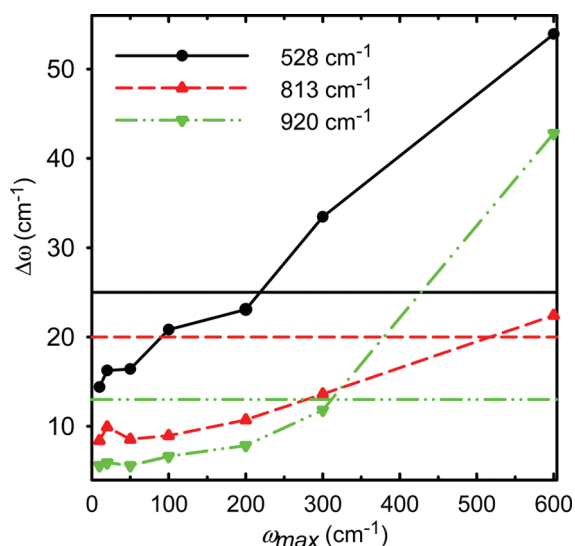


Figure 6. Simulated lactamide Raman bandwidths ($\Delta\omega$) as calculated for different ω_{max} for the bending (528 cm^{-1}), NH_2 wagging (813 cm^{-1}), and C–C/C–O stretching (920 cm^{-1}) vibrational modes. Experimental widths²⁸ are indicated by the horizontal lines.

narrower, adopting values mostly within $\sim 102^\circ$ – 130° for $\omega_{\text{max}} < 200 \text{ cm}^{-1}$. This reflects the intrinsic molecular potential driving motion of this angle. On the other hand, for χ_{OH} the dispersion ($\sim 200^\circ$ – 270° for nonoptimized clusters, and 210° – 290° for $\omega_{\text{max}} = 20 \text{ cm}^{-1}$) does not change much during the optimizations. This can be explained by the stabilizing effect of the surrounding water molecules that make hydrogen bonds to the OH group. The water positions do not change even for low values of ω_{max} .

The computed bandwidths for three nonoverlapping peaks with central frequencies at 528, 813, and 920 cm^{-1} are plotted in Figure 6 as obtained with the seven values of ω_{max} . The experimental widths, indicated by the horizontal lines, were lowered by 3 cm^{-1} to account for the instrument broadening. We consider this value to be a lower limit of the correction because of the instrument low-resolution setup optimized for ROA measurement, and the crude CCD detection of the wavenumbers where 1 pixel corresponds to about 3 cm^{-1} .

The comparison is also hampered by the experimental noise and transition overlap. Typically, each simulated band contains not only the dominant transition but also satellites. Nevertheless, in Figure 6, we can see that an optimal ω_{max} can be estimated at least approximately from the crossing of the simulated bandwidth curve with the experimental line, ranging from $\omega_{\text{max}} \sim 200 \text{ cm}^{-1}$ (for the 528 cm^{-1} band) to $\sim 500 \text{ cm}^{-1}$ (813 cm^{-1} band). A similar analysis of the ROA spectra and the direct Raman and ROA spectral comparison in Figure 3 suggest that an optimal ω_{max} value is close to the lower limit of the interval, within 200–300 cm^{-1} , curiously, this range comprises the Boltzmann temperature quantum ($kT \approx 208 \text{ cm}^{-1}$ at 300 K).

We think that a relation of the limit to kT is quite obvious for the reasons discussed above, although the actual empirical value found here may be a coincidence. Unfortunately, comparison with rigorous results, such as the VCI computation for the dimer, cannot be presently done for larger clusters to determine the relation more closely. On the other hand, the spectral profiles (cf. Figure 3) change very slowly with ω_{max} ; thus in a wide interval around the optimal value the spectra can be simulated realistically enough to allow for the normal-mode assignment and estimation of most of the solvent inhomogeneous normal-mode broadening.

CONCLUSIONS

The raw cluster simulations based on classical and ab initio molecular dynamics provide too wide vibrational bands and unrealistic geometry dispersion of the higher-frequency motions. On the two-dimensional model, we could show that this may be primarily caused by the coupling of vibrational modes and anharmonic force field terms. Geometries and, consequently, the effective harmonic normal-mode frequencies vary too much in the molecular dynamics trajectories. For the lactamide, we showed that the broadening of the vibrational bands simulated for an ensemble of clusters can be efficiently controlled by the normal mode optimization constraint. The resultant spectra exhibit not only better bandwidths but also relative intensities if compared to the experiment. The only empirical parameter, the cutoff of the vibrational frequencies in the constrained optimization, could be obtained by comparison of selected peaks in the experimental and simulated spectra. The empirical procedure of partial optimization could be to a large extent rationalized by the quantum properties of the vibrations, and provides an efficient means of modeling vibrational properties of molecules in solutions.

AUTHOR INFORMATION

Corresponding Author

*E-mail: bour@uochb.cas.cz.

ACKNOWLEDGMENT

The study was performed with support from the Academy of Sciences, Grant Agency of the Czech Republic (P208/11/0105),

the Grant Agency of Charles University (126310), the MSMT (LH11033), and Norwegian Supercomputing Program (Notur). We thank Prof. Kenneth Ruud for the discussion on this topic.

REFERENCES

- (1) Tomasi, J.; Mennucci, B.; Cammi, R. *Chem. Rev.* **2005**, *105*, 2999.
- (2) Mennucci, B.; Martínez, J. M. *J. Phys. Chem. B* **2005**, *109*, 9818.
- (3) Bouř, P.; Michalík, D.; Kapitán, J. *J. Chem. Phys.* **2005**, *122*, 144501.
- (4) Dračinský, M.; Kaminský, J.; Bouř, P. *J. Phys. Chem. B* **2009**, *113*, 14698.
- (5) Kamiya, N.; Watanabe, Y. S.; Ono, S.; Higo, J. *Chem. Phys. Lett.* **2005**, *401*, 312.
- (6) Car, R.; Parrinello, M. *Phys. Rev. Lett.* **1985**, *55*, 2471.
- (7) Lippert, G.; Hutter, J.; Parrinello, M. *Mol. Phys.* **1997**, *92*, 477.
- (8) Grimme, S.; Antony, J.; Ehrlich, S.; Krieg, H. *J. Chem. Phys.* **2010**, *132*, 154104.
- (9) Dračinský, M.; Bouř, P. *J. Chem. Theory Comput.* **2010**, *6*, 288.
- (10) Bouř, P.; Keiderling, T. A. *J. Chem. Phys.* **2003**, *119*, 11253.
- (11) Kaminský, J.; Bouř, P.; Kubelka, J. *J. Phys. Chem. A* **2011**, *115*, 30.
- (12) Yang, S.; Cho, M. *J. Chem. Phys.* **2005**, *123*, 134503.
- (13) Grahnen, J. A.; Amunson, K. E.; Kubelka, J. *J. Phys. Chem. B* **2010**, *114*, 13011.
- (14) Choi, J. H.; Kim, J. S.; Cho, M. *J. Chem. Phys.* **2005**, *122*, 174903.
- (15) Choi, J. H.; Cheon, S.; Lee, H.; Cho, M. *Phys. Chem. Chem. Phys.* **2008**, *10*, 3839.
- (16) Jeon, J.; Cho, M. *New J. Phys.* **2010**, *12*, 065001.
- (17) Miyazawa, T.; Blout, E. R. *J. Am. Chem. Soc.* **1961**, *83*, 712.
- (18) Krimm, S.; Bandekar, J. *Adv. Protein Chem.* **1986**, *38*, 181.
- (19) Torii, H.; Tatsumi, T.; Tasumi, M. *J. Raman Spectrosc.* **1998**, *29*, 537.
- (20) Kubelka, J.; Keiderling, T. A. *J. Phys. Chem. A* **2001**, *105*, 10922.
- (21) Barron, L. D. *Molecular Light Scattering and Optical Activity*; Cambridge University Press: Cambridge, UK, 2004.
- (22) Haesler, J.; Schindelholz, I.; Riguete, E.; Bochet, C. G.; Hug, W. *Nature* **2007**, *446*, 526.
- (23) Polavarapu, P. L. *Angew. Chem., Int. Ed.* **2002**, *41*, 4544.
- (24) Cheeseman, J. R.; Shaik, M. S.; Popelier, P. L. A.; Blanch, E. W. *J. Am. Chem. Soc.* **2011**, *133*, 4991.
- (25) Keyes, T. *J. Phys. Chem. A* **1997**, *101*, 2921.
- (26) Ahlborn, H.; Space, B.; Moore, P. B. *J. Chem. Phys.* **2000**, *112*, 8083.
- (27) Bouř, P. *Chem. Phys. Lett.* **2002**, *365*, 82.
- (28) Hopmann, K. H.; Ruud, K.; Pecul, M.; Kudelski, A.; Dračinský, M.; Bouř, P. *J. Phys. Chem. B* **2011**, *115*, 4128.
- (29) Kwac, K.; Lee, K. K.; Han, J.; Oh, K. I.; Cho, M. *J. Chem. Phys.* **2008**, *128*, 105106.
- (30) Gorbunov, R. D.; Nguyen, P. H.; Kobus, M.; Stock, G. *J. Chem. Phys.* **2007**, *126*, 054509.
- (31) Choi, J. H.; Lee, H.; Lee, K. K.; Hahn, S.; Cho, M. *J. Chem. Phys.* **2007**, *126*, 045102.
- (32) Joutsuka, T.; Ando, K. *J. Chem. Phys.* **2011**, *134*, 204511.
- (33) Bouř, P.; Keiderling, T. A. *J. Chem. Phys.* **2002**, *117*, 4126.
- (34) Bouř, P. *Collect. Czech. Chem. Commun.* **2005**, *70*, 1315.
- (35) Yamamoto, S.; Watarai, H.; Bouř, P. *ChemPhysChem* **2011**, *12*, 1509.
- (36) Andrushchenko, V.; Bouř, P. *J. Phys. Chem. A* **2007**, *111*, 9714.
- (37) Papoušek, D.; Aliev, M. R. *Molecular Vibrational/Rotational Spectra*; Academia: Prague, 1982.
- (38) Becke, A. D. *J. Chem. Phys.* **1993**, *98*, 5648.
- (39) Frisch, M. J.; Trucks, G. W.; Schlegel, H. B.; Scuseria, G. E.; Robb, M. A.; Cheeseman, J. R.; Scalmani, G.; Barone, V.; Mennucci, B.; Petersson, G. A.; Nakatsuji, H.; Caricato, M.; Li, X.; Hratchian, H. P.; Izmaylov, A. F.; Bloino, J.; Zheng, G.; Sonnenberg, J. L.; Hada, M.; Ehara, M.; Toyota, K.; Fukuda, R.; Hasegawa, J.; Ishida, M.; Nakajima, T.;

Honda, Y.; Kitao, O.; Nakai, H.; Vreven, T.; Montgomery, J., J. A.; Peralta, J. E.; Ogliaro, F.; Bearpark, M.; Heyd, J. J.; Brothers, E.; Kudin, K. N.; Staroverov, V. N.; Kobayashi, R.; Normand, J.; Raghavachari, K.; Rendell, A.; Burant, J. C.; Iyengar, S. S.; Tomasi, J.; Cossi, M.; Rega, N.; Millam, J. M.; Klene, M.; Knox, J. E.; Cross, J. B.; Bakken, V.; Adamo, C.; Jaramillo, J.; Gomperts, R.; Stratmann, R. E.; Yazyev, O.; Austin, A. J.; Cammi, R.; Pomelli, C.; Ochterski, J. W.; Martin, R. L.; Morokuma, K.; Zakrzewski, V. G.; Voth, G. A.; Salvador, P.; Dannenberg, J. J.; Dapprich, S.; Daniels, A. D.; Farkas, O.; Foresman, J. B.; Ortiz, J. V.; Cioslowski, J.; Fox, D. J. *Gaussian 09, Revision A.02*; Gaussian, Inc.: Wallingford, CT, 2009.

- (40) Barone, V. J. *Phys. Chem. A* **2004**, *108*, 4146.
- (41) Daněček, P.; Bouř, P. *J. Comput. Chem.* **2007**, *28*, 1617.
- (42) Bouř, P. *S4, program for anharmonic vibrational properties*; Academy of Sciences: Prague, 2010.
- (43) Peng, C.; Ayala, P. Y.; Schlegel, H. B.; J., F. M. *J. Comput. Chem.* **1996**, *17*, 49.
- (44) Pulay, P.; Fogarasi, G. *J. Chem. Phys.* **1992**, *96*, 2856.
- (45) Bouř, P. *Qgrad*; Academy of Sciences, Prague: Prague, 2006.
- (46) Broyden, C. G. *J. Inst. Math. Appl.* **1970**, *6*, 76.
- (47) Fletcher, R. *Comput. J.* **1970**, *13*, 317.
- (48) Goldfarb, D. *Math. Comput.* **1970**, *24*, 23.
- (49) Shanno, D. F. *Math. Comput.* **1970**, *24*, 647.
- (50) Schlegel, H. B. Geometry optimization on potential energy surfaces. In *Modern electronic structure theory*; Yarkony, D. R., Ed.; World Scientific: Singapore, 1995; p 459.
- (51) Banerjee, A.; Adams, N.; Simons, J.; Shepard, R. *J. Phys. Chem.* **1985**, *89*, 52.
- (52) Simons, J.; Nichols, J. *Int. J. Quantum Chem., Quantum Chem. Symp.* **1990**, *24*, 263.
- (53) Baker, J.; Hehre, W. J. *J. Comput. Chem.* **1991**, *12*, 606.
- (54) Baker, J. *J. Comput. Chem.* **1993**, *14*, 1085.
- (55) Polavarapu, P. L. *Vibrational spectra: principles and applications with emphasis on optical activity*; Elsevier: Amsterdam, 1998; Vol. 85.
- (56) Buděšínský, M.; Daněček, P.; Bednářová, L.; Kapitán, J.; Baumruk, V.; Bouř, P. *J. Phys. Chem. A* **2008**, *112*, 8633.
- (57) Daněček, P.; Kapitán, J.; Baumruk, V.; Bednářová, L.; Kopecký, V., Jr.; Bouř, P. *J. Chem. Phys.* **2007**, *126*, 224513.